

RESEARCH ARTICLE | JANUARY 25 2006

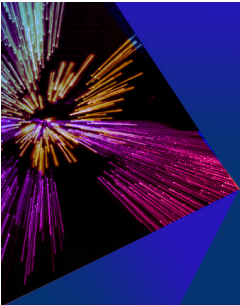
Inelastic Takahashi hard-rod gas

Umberto Marini-Bettolo-Marconi; Maurizio Natali; Giulio Costantini; Fabio Cecconi




J. Chem. Phys. 124, 044507 (2006)

<https://doi.org/10.1063/1.2161215>





The Journal of Chemical Physics



**Special Topic: Festschrift in
honor of Yuen-Ron Shen**

Submit Today



Inelastic Takahashi hard-rod gas

Umberto Marini-Bettolo-Marconi, Maurizio Natali, and Giulio Costantini

Dipartimento di Fisica, Università di Camerino, Via Madonna delle Carceri, I-62032 Camerino, Italy

Fabio Cecconi^{a)}

INFN and Istituto dei Sistemi Complessi (ISC-CNR), Via dei Taurini 19, I-00185 Roma, Italy

(Received 4 August 2005; accepted 1 December 2005; published online 25 January 2006)

We study a one-dimensional fluid of hard rods interacting with each other via binary inelastic collisions and a short-ranged square-well potential. Upon tuning the depth and the sign of the well, we investigate the interplay between dissipation and cohesive or repulsive forces. Molecular-dynamics simulations of the cooling regime indicate that the presence of this simple interparticle interaction is sufficient to significantly modify the energy dissipation rates expected by Haff's law for the free cooling. The simplicity of the model makes it amenable to an analytical approach based on the Boltzmann-Enskog transport equation which allows deriving the behavior of the granular temperature. Furthermore, in the elastic limit, the model can be solved exactly to provide a full thermodynamic description. A meaningful theoretical approximation explaining the properties of the inelastic system in interaction with a thermal bath can be directly extrapolated from the properties of the corresponding elastic system, upon a proper redefinition of the relevant observables. Simulation results both in the cooling and driven regimes can be fairly interpreted according to our theoretical approach and compare rather well to our predictions. © 2006 American Institute of Physics. [DOI: [10.1063/1.2161215](https://doi.org/10.1063/1.2161215)]

I. INTRODUCTION

Granular materials are ubiquitous in nature and their handling occurs in many types of industrial activities. While they are very common, their properties often are not. In the last 20 years there has been a great progress in the comprehension of static and dynamical properties of granular flows.^{1–5} In spite of the fact that most of the theoretical research in this context has been based on the inelastic hard-sphere model, several observations suggest that neither cohesive forces⁶ nor electrostatic repulsion⁷ can be ignored. Understanding how simple interactions modify the behavior of a granular gas can have important practical consequences. Cohesive forces have to be considered when studying wet granular matter: the humidity may lead to the formation of thin layers of water on the surface of the grains and induce adhesion through capillarity effects. The presence of liquid-vapor interfaces can enhance the mechanical stability of an assembly of grains, as illustrated by sand castles.⁸ On the other side, repulsive forces also play a role, as stressed by Sheffler and Wolf.⁷ Dry granular materials tend to become electrically charged due to contact electrification during transport. In the case of monopolar charging the particles experience mutual Coulombic repulsion. Finally, Blair and Kudrolli⁹ studied the behavior of a vibrated system of magnetic grains, where forces of tensorial character are in action, and found coexistence of long-lived clusters with isolated particles. Clusters can manifest as chains or globular structures according to the driving intensity.

In this work we introduce and study a one-dimensional model which can be tuned to describe both the cohesive and

the repulsive regime. One-dimensional models have often been employed in the literature^{10–14} to study granular fluids because their simplicity provides a valuable testing ground for theoretical approaches and approximations. Our model consists of a set of inelastic hard rods subjected to square-well potential, as shown in Fig. 1. The attractive potential mimics the action of cohesive forces responsible for adhesion among particles which are crucial effects when considering fine particulates such as powders or sands. On the contrary, the barrier describes the effect of soft materials which may present a deformable shell covering the hard-core nucleus.

The choice of a square-well interparticle interaction is particularly convenient in a computer implementation of the model since it reduces Newton's equations to algebraic expressions. Indeed, in the cooling regime, rods move with constant velocity until they pass a barrier or their cores touch. Thus the collisional cooling can be simulated through the collision driven algorithm of Alder and Wainwright.¹⁵ We shall analyze the interplay between the potential and the collisional dissipation typical of granular materials. In particular, we discuss the influence of the square-well interaction on the rate of energy dissipations in the same spirit of reference.⁷ It is well known that in the homogeneous free cooling process, a system of inelastic hard spheres dissipates its kinetic energy at a rate proportional to the square root of the kinetic temperature, T , the so-called granular temperature, and that T decreases in time as the inverse of square time.¹⁶ As we shall see, this picture is partially modified by the presence of a short-range repulsive or attractive potential barrier. By treating collisions according to Enskog's equation, a generalization of Boltzmann equation to dense-fluid

^{a)}Electronic mail: cecconif@roma1.infn.it

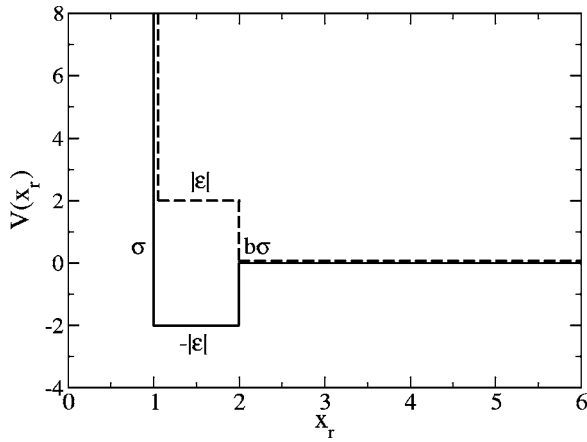


FIG. 1. Sketch of the interaction potential Eq. (1) as a function of the interparticle distance x_r , for $b=2$ and $\sigma=1$. Solid line refers to attraction ($\epsilon > 0$) while dashed to repulsion ($\epsilon < 0$).

regime, we are able to make some predictions about the cooling behavior of the model. In addition we consider its properties when it is kept in contact to a stochastic source of energy which balances the energy loss due to inelastic collisions. In this case, the system reaches a steady regime whose properties can be partly understood through a direct comparison with the properties of corresponding elastic system.

The paper is organized as follows. Section II describes the model we use and the main features of the simulations and technical details. Section III shows the thermodynamics of the elastic version of the model in order to have a reference system to compare inelastic results. In Sec. IV, an analytic estimate of granular temperature of the system is derived through a Boltzmann-Enskog approach. Section V illustrates simulation results of the inelastic model both in the cooling and driven regimes with a comparison with theoretical predictions. Finally Sec. VI contains a brief discussion and conclusions.

II. THE MODEL

We consider N identical impenetrable rods of mass $m = 1$, size $\sigma = 1$, and positions $x_i(t)$ and velocities $v_i(t)$ constrained to move in a periodic domain of size L . They interact through a potential $V(|x_i - x_j|)$ consisting of a hard-rod part and a square-well potential, as shown in Fig. 1. Explicitly, we consider

$$V(x) = \begin{cases} \infty & \text{if } x < \sigma \\ -\epsilon & \text{if } \sigma \leq x \leq b\sigma \\ 0 & \text{if } x > b\sigma, \end{cases} \quad (1)$$

where the parameter b defines the characteristic range of the interaction. The effect of a piece-wise constant potential $V(x)$ amounts to a set of simple collision rules, similar to those involved in the dynamics of hard rods. Several kinds of collisions between two neighbor particles may occur when their distance is

$$\Delta x_i(t) \equiv x_{i+1}(t) - x_i(t) = b\sigma.$$

If $\epsilon > 0$ the following cases are possible: (I) particles entering the well, (II) particles leaving the well, and (III) particles

being trapped and rebounding at the inside square-well edge, because their relative kinetic energy is not sufficient to escape.

On the other hand, if $\epsilon < 0$ one has the cases: (I') particles overcoming the repulsive barrier [$m(v_i - v_{i+1})^2 > 4|\epsilon|$], (II') particles descending the barrier, and (III') particles being repelled by the barrier, when $m(v_i - v_{i+1})^2 < 4|\epsilon|$.

The postcollisional velocities in cases III and III' are given by

$$v'_i = v_{i+1},$$

$$v'_{i+1} = v_i.$$

In the remaining cases the collision rules are found by requiring again the conservation of the total energy and total momentum at the edge of the square-well potential. If particles are entering [$s_i \equiv \text{sgn}(v_i - v_{i+1}) > 0$], while if they are leaving the well ($s_i < 0$), and the collision rule reads

$$\begin{aligned} v'_i &= \frac{(v_i + v_{i+1})}{2} + s_i \sqrt{\frac{(v_i - v_{i+1})^2}{4} + s_i \frac{\epsilon}{m}}, \\ v'_{i+1} &= \frac{(v_i + v_{i+1})}{2} - s_i \sqrt{\frac{(v_i - v_{i+1})^2}{4} + s_i \frac{\epsilon}{m}}, \end{aligned} \quad (2)$$

where precollisional and postcollisional velocities are indicated by unprimed and primed symbols, respectively.

We finally consider the hard-core inelastic collision at

$$\Delta x_i(t) \equiv x_{i+1}(t) - x_i(t) = \sigma,$$

which results in the transformation

$$v'_{i+1} = v_{i+1} - \frac{1 + \alpha}{2}(v_{i+1} - v_i), \quad (3)$$

$$v'_i = v_i + \frac{1 + \alpha}{2}(v_{i+1} - v_i),$$

where α indicates a constant coefficient of restitution and $0 \leq \alpha \leq 1$.

Besides impulsive forces between particles, we shall also consider an external stochastic white-noise force, whose role is to fluidize the system and balance the energy losses due to dissipative forces. The dynamics between two consecutive collisions is described by the following Langevin equation:

$$m \frac{d^2 x_i(t)}{dt^2} = -m\gamma \frac{dx_i(t)}{dt} + \xi_i, \quad (4)$$

where $-m\gamma dx_i/dt$ is a viscous term and ξ_i is a Gaussian random force, with zero average and variance satisfying a fluctuation-dissipation relation,

$$\langle \xi_i(t) \xi_j(t') \rangle = 2m\gamma T \delta_{ij} \delta(t - t'), \quad (5)$$

with T proportional to the intensity of the stochastic driving.^{17,18} The damping term renders the system stationary even in the absence of collisional dissipation and physically can represent the friction between the particles and the container. Summarizing, the position x_i ($i = 1, N$) of the i th particle evolves according to the equation

$$m \frac{d^2 x_i(t)}{dt^2} = -m\gamma \frac{dx_i(t)}{dt} + \xi_i(t) + \sum_j f_{ij}(t), \quad (6)$$

where f_{ij} indicates the resultant of impulsive forces between particles i and j . Since the dynamics of the model is mainly ruled by impulsive forces, molecular-dynamics (MD) simulations make use of a collision driven algorithm.

III. ELASTIC SYSTEM: EQUILIBRIUM PROPERTIES

The elastic fluid, corresponding to the limit $\alpha=1$ in Eq. (3), serves conveniently as a reference system. Thus, we consider its equilibrium properties, that we shall compare to properties of the stationary inelastic system to build a theoretical approach valid in the region of moderate inelasticity. The equilibrium square-well fluid model is exactly solvable when the interaction range is restricted to first neighbors, i.e., $b \leq 2$, the excluded volume allows no more than two particles to experience the same potential well. In that case, the Gibbs free energy, $G(P, T, N)$, can be derived using the isothermal-isobaric ensemble.^{19,20} Here, the partition function $Y(P, T, N)$ is related to that of the one-dimensional canonical ensemble $Z(T, L, N)$ by

$$Y(P, T, N) = \frac{1}{\Lambda^N \Lambda_0} \int_0^\infty dL e^{-\beta PL} Z(T, L, N), \quad (7)$$

where P is the thermodynamic pressure, $\Lambda \equiv h/\sqrt{2\pi mk_B T}$ is the temperature-dependent de Broglie wavelength, and Λ_0 is an arbitrary constant with dimension of a length.

Following the existing literature,²⁰ the isothermal-isobaric partition function for N rods of length σ can be written as

$$Y(P, T, N) = \frac{\Lambda}{\Lambda_0} \left\{ \frac{1}{\beta P \Lambda} [e^{\beta \epsilon} (e^{-\beta P \sigma} - e^{-\beta P b \sigma}) + e^{-\beta P b \sigma}] \right\}^{N+1}. \quad (8)$$

The associated Gibbs potential,

$$G(P, T, N) = -\frac{1}{\beta} \ln Y(P, T, N),$$

reads a part from a constant

$$G(P, T, N) = (N+1) \left\{ b\sigma P + \frac{1}{\beta} \ln(\beta P \Lambda) - \frac{1}{\beta} \ln[1 + e^{\beta \epsilon} (e^{\beta P (b-1)\sigma} - 1)] \right\}. \quad (9)$$

The equation of state, relating density, pressure, and temperature, is obtained by differentiating G with respect to P and defining the ‘‘volume’’ per particle, $\rho^{-1} = \bar{L}/N$, of the system,

$$\frac{1}{\rho} = b\sigma + \frac{1}{\beta P} - \frac{(b-1)\sigma}{1 + e^{-\beta P (b-1)\sigma} (e^{-\beta \epsilon} - 1)}, \quad (10)$$

that can be recast to the more familiar form

$$\frac{\beta P}{\rho} = \frac{1}{1 - \rho \sigma B}, \quad (11)$$

with

$$B = \frac{1 + b e^{-\beta P (b-1)\sigma} (e^{-\beta \epsilon} - 1)}{1 + e^{-\beta P (b-1)\sigma} (e^{-\beta \epsilon} - 1)}.$$

Notice that $b=1$ implies $B \rightarrow 1$, therefore the hard-rod pressure is straightforwardly recovered.

In order to apply Enskog’s kinetic approach, we need to compute the equilibrium pair-correlation function in the thermodynamic limit. The pair correlation is defined as

$$\rho g(y) \equiv \sum_{r=1}^{\infty} \langle \delta(x_{l+r} - x_l - y) \rangle. \quad (12)$$

To perform the average in Eq. (12), we represent the delta distribution (with $l=1$ and $q=r+l$) by its Fourier transform

$$\delta(x_q - x_1 - y) \equiv \int_{-\infty}^{\infty} \frac{dk}{2\pi} \exp[ik(x_q - x_1 - y)], \quad (13)$$

and write the average explicitly in terms of the Boltzmann weights $f(x) = \exp[-\beta V(x)]$,

$$\begin{aligned} & \langle \delta(x_q - x_1 - y) \rangle \\ &= \frac{1}{Z(T, L, N)} \int_{-\infty}^{\infty} \frac{dk}{2\pi} e^{-iky} \int_0^L dx_q \int_0^{x_q} dx_{q-1} \cdots \int_0^{x_2} dx_1 \\ & \quad \times f(L - x_q) f(x_q - x_{q-1}) \cdots f(x_2 - x_1) f(x_1) e^{ik(x_q - x_1)}. \end{aligned} \quad (14)$$

Since the last expression has the form of an iterated convolution, one can obtain the desired average by means of standard Laplace transform method, a simple generalization of the method²⁰ employed to compute $Z(T, L, N)$ in the isothermal-isobaric ensemble. After a lengthy calculation, in the thermodynamic limit $N \rightarrow \infty$ and constant pressure, we get the series

$$\rho g(y) = \sum_{r=1}^{\infty} \frac{A_r(y)}{(r-1)!} \frac{(\beta P)^r e^{-\beta P y}}{[e^{\beta \epsilon} (e^{-\beta P \sigma} - e^{-\beta P b \sigma}) + e^{-\beta P b \sigma}]^r}, \quad (15)$$

where the coefficients can be written as

$$\begin{aligned} A_r(y) &= \sum_{k=0}^r \binom{r}{k} \Theta[y - \sigma(r + (b-1)k)] \\ & \quad \times [y - \sigma(r + (b-1)k)]^{r-1} (1 - e^{\beta \epsilon})^k (e^{\beta \epsilon})^{r-k}, \end{aligned} \quad (16)$$

where $\Theta(x)$ is the unitary step function.²¹ Notice that for a pure hard-rod system [$\epsilon=0$, $\beta P = \rho/(1 - \rho\sigma)$], one finds

$$\begin{aligned} \rho g_{hr}(y) &= \sum_{r=1}^{\infty} \frac{1}{(r-1)!} \frac{\rho^r}{(1 - \rho\sigma)^r} \Theta(y - r\sigma) (y - r\sigma)^{r-1} \\ & \quad \times \exp\left[-\frac{\rho}{1 - \rho\sigma} (y - r\sigma)\right], \end{aligned} \quad (17)$$

a result which agrees with the well known result by Zernike and Prins.^{22,23} From expressions (15) and (16), the value of the pair correlation at contact can be extracted explicitly,

$$g(\sigma) = \frac{\beta P}{\rho} \frac{1}{1 + e^{-\beta P(b-1)\sigma}(e^{-\beta\epsilon} - 1)}. \quad (18)$$

Since the thermodynamic pressure can be expressed in terms of $g(x)$ through the virial equation²⁴

$$\frac{\beta P}{\rho} = 1 - \frac{\beta \rho}{2} \int_{-\infty}^{\infty} dx V'(x) x g(x), \quad (19)$$

after some rearrangements, the pressure reads

$$\frac{\beta P}{\rho} = 1 + \rho \sigma [g(\sigma) + b g(b\sigma^+) - b g(b\sigma^-)], \quad (20)$$

where the discontinuity of the potential (1) at $x=b\sigma$ results in a jump of the binary correlation function,

$$g(b\sigma^+) = g(\sigma) e^{-\beta P(b-1)\sigma - \beta\epsilon}, \quad (21)$$

$$g(b\sigma^-) = g(\sigma) e^{-\beta P(b-1)\sigma}, \quad (22)$$

with $g(b\sigma^\pm) = \lim_{\delta \rightarrow 0} g(b\sigma \pm \delta)$. These relations are consistent with Eq. (10) and show that the pressure depends not only on the value of the pair correlation at contact, but also on its values at $x=b\sigma$.

IV. BOLTZMANN-ENSKOG EQUATION

The system dynamics is determined by the combined effects of the heat-bath and interparticle collisions. Thus, the one-particle phase distribution function $f(x, v, t)$, in the absence of external drift and large density fluctuations, evolves under the action of a Kramers operator associated with the interaction with the heat bath,

$$\mathcal{L}_K = \frac{\gamma}{m\beta} \frac{\partial^2}{\partial v^2} + \gamma \frac{\partial}{\partial v} v,$$

plus a collision operator that we represent for the sake of simplicity as a Boltzmann-Enskog collision integral,

$$\frac{\partial f(v, t)}{\partial t} = \mathcal{L}_K f(v, t) + I(v, t). \quad (23)$$

Adapting to the present case arguments^{25,26} similar to those leading to the derivation of the standard Enskog theory (SET) we arrive at the following form of the Boltzmann-Enskog collision integral $I(v, t)$:

$$I(v, t) = I_0(v, t) + I_+(v, t) + I_-(v, t) + I_{BS}(v, t), \quad (24)$$

where the four contributions represent, respectively,

- the inelastic hard-core collision,

$$I_0(v, t) = g(\sigma) \int dv' \int dv'' |v' - v''| \times f(v') f(v'') \times \left\{ \delta \left[v - \frac{1-\alpha}{2} v' - \frac{1+\alpha}{2} v'' \right] - \delta[v - v''] \right\}, \quad (25)$$

- the entering collision $[(v' - v'') > 0]$,

$$I_+(v, t) = g(b\sigma^+) \int dv' \int dv'' \Theta \left[(v' - v'')^2 + \frac{4\epsilon}{m} \right] \times \left\{ \delta \left[v - \frac{v' + v''}{2} + \sqrt{\frac{(v' - v'')^2}{4} + \frac{\epsilon}{m}} \right] - \delta[v - v''] \right\} |v' - v''| f(v') f(v''), \quad (26)$$

- the escape collision $[(v' - v'') < 0]$,

$$I_-(v, t) = g(b\sigma^-) \int dv' \int dv'' \Theta \left[(v' - v'')^2 - \frac{4\epsilon}{m} \right] \times \left\{ \delta \left[v - \frac{v' + v''}{2} - \sqrt{\frac{(v' - v'')^2}{4} - \frac{\epsilon}{m}} \right] - \delta[v - v''] \right\} |v' - v''| f(v') f(v''), \quad (27)$$

- the elastic bound-state collision at $\Delta x = b\sigma^-$,

$$I_{BS}(v, t) = 0,$$

which in one dimension vanishes and therefore can be omitted.

We can apply the previous analysis to the theoretical description of the cooling process in the presence of the interparticle potential, under the hypothesis of spatial homogeneity. By integrating with respect to v the second term in the right-hand side of Eqs. (25)–(27) and approximating $f(v)$ with Maxwellian distribution of temperature T_g , we obtain the Enskog collision frequency at $\Delta x = \sigma$, and the frequencies of entering and escaping collisions,

$$\begin{aligned} \omega_0(\rho\sigma) &= \langle |v_{\text{rel}}| \rangle \rho g(\sigma), \\ \omega_+(\rho\sigma) &= \langle |v_{\text{rel}}| \rangle \rho g(b\sigma^+) [\Theta(\epsilon) + \Theta(-\epsilon) e^{\beta\epsilon}], \\ \omega_-(\rho\sigma) &= \langle |v_{\text{rel}}| \rangle \rho g(b\sigma^-) [\Theta(-\epsilon) + \Theta(\epsilon) e^{-\beta\epsilon}]. \end{aligned} \quad (28)$$

The expression for ω_0 is formally identical to that obtained in the case of simple hard rods without potential tail. It can be easily verified that the two factors containing the Θ functions are exactly the terms that compensate the asymmetry coming from expressions (21) and (22). Therefore, the rates become equal,

$$\omega_+ = \omega_- = \begin{cases} \langle |v_{\text{rel}}| \rangle \rho g(\sigma) e^{-\beta P(b-1)\sigma} & \text{if } \epsilon < 0 \\ \langle |v_{\text{rel}}| \rangle \rho g(\sigma) e^{-\beta P(b-1)\sigma - \beta\epsilon} & \text{if } \epsilon > 0, \end{cases} \quad (29)$$

and thus satisfy a detailed balance relation between entering and escape collisions. The presence of the potential is reflected in the modified value of the pair correlation at contact, Eq. (18). By substituting $\langle |v_{\text{rel}}| \rangle = 2(\beta\pi m)^{-1/2}$ we find the following expression for the collision time of the square-well fluid:

$$\omega_0 = 2 \sqrt{\frac{\beta}{\pi m}} \frac{P}{1 + e^{-\beta P(b-1)\sigma}(e^{-\beta\epsilon} - 1)}. \quad (30)$$

For the sake of comparison the hard-rod Enskog frequency reads

$$\omega_{hr} = 2 \sqrt{\frac{\beta}{\pi m}} P_{hr}, \quad (31)$$

with $\beta P_{hr} = \rho / (1 - \rho\sigma)$.

Interestingly, in an elastic system with repulsive forces, the ratio between the hard-core collision frequency and the entering/escape frequency reads

$$\frac{\omega_0}{\omega_{\pm}} = e^{\beta P(b-1)\sigma}, \quad (32)$$

it suggests that at high densities hard-core collisions dominate, because the pressure is a growing function of the density. Therefore, increasing the density amounts somehow to lowering the height of the effective potential barrier, i.e., the kinetic energy required to perform an elastic collision.

We now consider, how the average kinetic energy of the inelastic system ($\alpha < 1$) is dissipated. By multiplying Eq. (24) by v^2 and integrating over the velocity, we can compute the loss of kinetic energy due to collisions. Since only hard-core collisions dissipate energy we find that solely the process represented by Eq. (25) contributes to the evolution equation²⁷ for the granular temperature $T_g(t)$,

$$\frac{dT_g}{dt} = -(1 - \alpha^2)\omega_0 T_g. \quad (33)$$

Notice that the expression (30) for ω_0 , entering Eq. (33), employs a pair-correlation function $g(\sigma)$ extrapolated from its equilibrium value, where β has been identified with the inverse granular temperature, i.e., $\beta = 1/T_g$. Moreover, the value of the pressure necessary to compute the frequency ω_0 can be obtained numerically by inverting Eq. (10) for a given density of the system. The rate ω_0 decreases with increasing the repulsive barrier ($\epsilon \rightarrow -\infty$) or when the temperature tends to zero. Consequently, as the system cools down, the dissipation rate will be much slower than the corresponding rate when $\epsilon = 0$.

V. NUMERICAL RESULTS

Whereas the equilibrium properties of the conservative system are analytically accessible, most of the properties of its dissipative version need MD simulations to be investigated. After resorting to numerical methods we shall compare their results with our theoretical estimates. At values of the restitution parameter α less than 1, the system is certainly not in thermodynamic equilibrium, but can achieve a stationary state when in contact with the heat bath described by Eq. (5).

We shall consider the behavior of the system both in the cooling regime ($\gamma = 0$ and $T = 0$) and in the stationary heated regime. The numerical methods employed have been briefly mentioned in the previous section and described in detail in papers^{28,29} which the reader can refer to.

In order to minimize surface effects and simulate an infinite system, periodic boundary conditions are imposed on the equations of motion. During each simulation run, we monitor the kinetic temperature, named granular temperature, T_g , which by definition is proportional to the average of the kinetic energy per particle,

$$T_g = \frac{1}{N} \sum_i^N m[\langle v_i^2 \rangle - \langle v_i \rangle^2], \quad (34)$$

having chosen units in which $k_B = 1$. The values of pressure, instead, can be obtained from the virial formula³⁰ properly modified for the present system,

$$\frac{PL}{NT_g} = 1 + \frac{1 + \alpha}{2} \frac{m}{t_{ob} NT_g} Z, \quad (35)$$

where Z indicates the sum,

$$Z = \sum_{\text{all coll}} x_{ij} v_{ij}, \quad (36)$$

where t_{ob} is the observation time and $x_{ij} = (x_i - x_j)$ and $v_{ij} = (v_i - v_j)$ are, respectively, the separation and the relative velocity at the moment of collision. Both kinds of collisional events $|x_{ij}| = \sigma$ and $|x_{ij}| = b\sigma$ determine an exchange of momenta among the particles.

A. Cooling regime

We consider, first, the properties of a system of $N = 2000$ particles evolving without the presence of heat bath, thus no energy injection ($T = 0$) and no friction ($\gamma = 0$) occur. In the literature this situation is generally referred to as free cooling. The properties of this system with $\epsilon = 0$ have been studied thoroughly^{10–14,31,32} and are well known. Due to the repeated inelastic collisions, the temperature T_g decreases and after a short transient, lasting only few collisions per particle, T_g displays the typical power-law behavior t^{-2} , known as Haff's law. During such a regime, the density remains homogeneous and the velocity distribution converges, from the initial Maxwellian, to a two-hump function. As the system cools down, particles cluster into two "streams" at the outer edges the distribution and a bimodal velocity distribution emerges.

Our MD simulations show that this scenario is modified by the presence of potential tail [see Eq. (1)]. Every MD run starts from an initial state characterized by $N = 2000$ particles with a Maxwellian velocity distribution of temperature T and uniformly distributed in space with no overlaps. During the dynamics, the grains spontaneously organize toward a state where the velocity distribution $P(v)$ depends on the attractive or repulsive character of $V(x)$. The behavior of $P(v)$ is clearly shown in Fig. 2, where later time distributions are characterized by a nearly Gaussian shape for $\epsilon > 0$ and no longer Gaussian for $\epsilon < 0$. The attractive interaction has the effect to accelerate the dissipation, however, the velocity distribution does not display the typical two-hump feature proper of the $\epsilon = 0$ case, remaining a single peak function of shrinking width (see Fig. 2, left panel).

On the contrary, when the potential is repulsive, only those pairs with velocities satisfying the condition $(v_i - v_{i+1})^2 > 4|\epsilon|/m$ may perform inelastic collisions. Such a selection mechanism is irrelevant when $T_g \gg \epsilon$, i.e., the very early stages of the simulations, however, it eventually leads to velocity distributions with small tails outside the region $-\sqrt{|\epsilon|/m} \leq v \leq \sqrt{|\epsilon|/m}$ and almost flat inside (Fig. 2, right

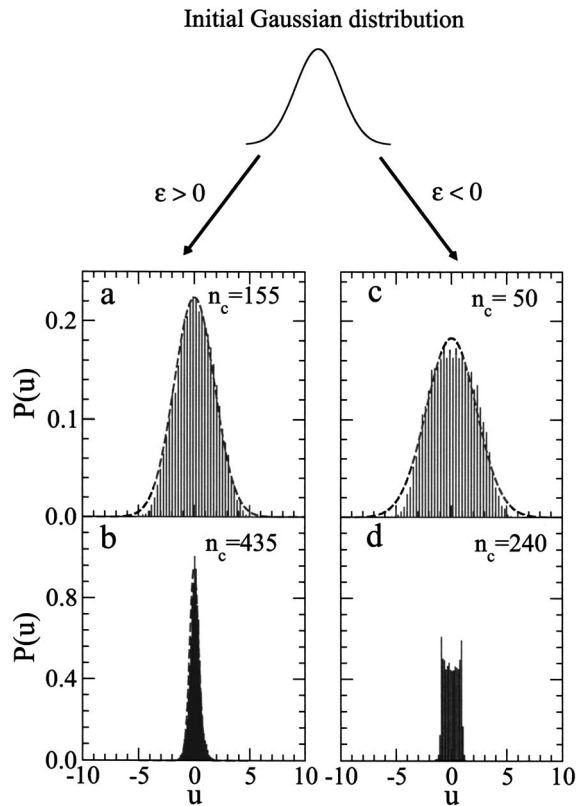


FIG. 2. Quenching of particle velocities observed at two stages of the cooling process of a system with attractive ($\epsilon=1$, left) and repulsive ($\epsilon=-1$, right) interparticle interactions. The histograms of the rescaled (dimensionless) velocity $u = v\sqrt{m/|\epsilon|}$ are collected after n_c hard-core collisions per particle have occurred. Simulations refer to a system of $N=2000$ particles and parameters $\alpha=0.99$, $\rho\sigma=0.002$, and $b=2$. The Gaussian fits (dashed lines) are plotted for comparison.

panel). Two small peaks can also be observed at $v = \pm\sqrt{|\epsilon|/m}$, likely, a reminiscence of the free-cooling two stream mechanism.

Equation (30) indicates that, under repulsive interaction, particles collide inelastically with an initial rate $\omega_0 \propto \sqrt{T_g}$, that, as the system cools down, makes the crossover to the behavior $\omega_0 \propto \sqrt{T_g} \exp(\epsilon/T_g)$. Accordingly, fewer and fewer particle pairs will collide and the cooling slows down leading to a logarithmic decay in time of the temperature. However, this argument turns out to be incorrect. Indeed, Fig. 3 proves that the energy dissipation process occurs with a slower time decay than the prediction given by Eq. (33). The direct comparison between theoretical and simulated dimensionless rate $R = \tau \dot{T}_g / T_0$ is shown in the inset, where τ is a proper time scale. The reason for such a discrepancy relies on the fact that the Maxwellian approximation for the velocity distributions, used to derive the rate expression (30), fails as it seen from Fig. 2 (right). With the actual shape of the distribution $P(v)$, indeed, the system dissipates only a negligible fraction of the kinetic energy and undergoes an effective reelasticization, implying that the non-Maxwellian character of $P(v)$ is maintained up to the inelastic collapse. Our theoretical estimate of the collision frequencies works better at moderate densities, where dissipation can counterbalance the reelasticization. As it suggested by Eq. (32) indeed, the pressure

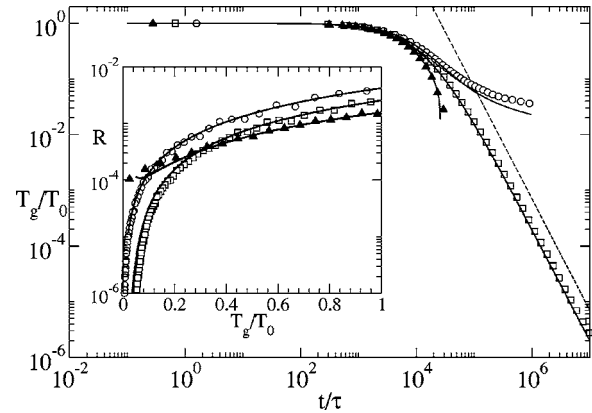


FIG. 3. Simulation results of the energy decay with time measured units $\tau = \sigma\sqrt{m/T_0}$, for $\epsilon=0$ (squares), $\epsilon=-1$ (circles), and $\epsilon=1$ (triangles) at effective density $\rho\sigma=0.002$. Each point is the average over 100 trajectories of a system with $N=2000$ hard rods and initial temperature $T_0=10$. The lines represent the analytical estimate from Eqs. (30) and (33), coherently with Eq. (10). Inset: plot of the theoretical and numerical (dimensionless) dissipation rates $R = \tau \dot{T}_g$ vs the rescaled granular temperature (same symbols).

exerted by the dense surrounding fluid on two colliding partners may overwhelm their repulsion, so that they will experience frequent hard-core collisions, i.e., $\omega_0 \gg \omega_{\pm}$.

B. Driven regime

The scenario changes when the system is coupled to a heat bath at temperature T . A steady regime, characterized by almost constant granular temperature and pressure, is attained. As already done for the cooling regime, we can derive an implicit relation for T_g (Refs. 28 and 29) by multiplying both sides of Eq. (23) by v^2 and integrating with respect to v ,

$$\left[1 + (1 - \alpha^2) \frac{\omega_0(T_g)}{2\gamma} \right] T_g = T. \quad (37)$$

The variation of T_g with density, given by the numerical solution of Eq. (37), is compared in Fig. 4 with the results of

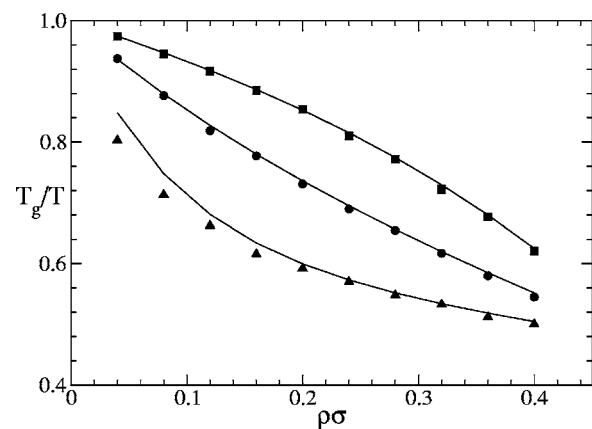


FIG. 4. Dependence of the ratio between granular T_g and bath temperature $T=10$ on the density, for a system with repulsive $\epsilon=-10$ (squares), vanishing $\epsilon=0$ (circles), and attractive $\epsilon=10$ (triangles) interparticle interactions. The points indicate the average over a set of 10^4 samplings in a single MD run of duration $t_{\max}=10^4$. The solid lines refer to theoretical temperatures extracted from the numerical solution of Eq. (37). The number of particles is $N=2000$, the remaining parameters are chosen as $\alpha=0.9$, $\gamma=0.2$, and $b=2$.

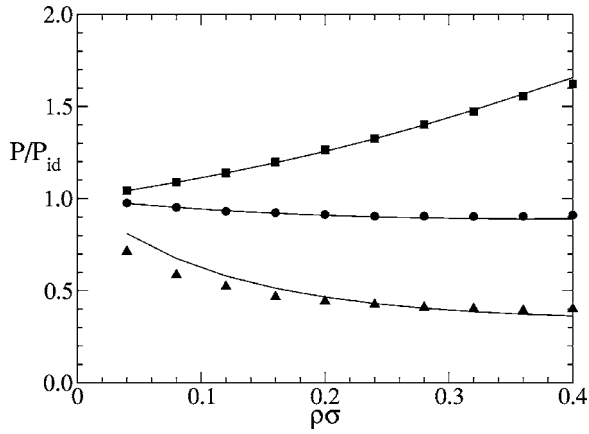


FIG. 5. Pressure of an inelastic system, rescaled to the equivalent ideal gas pressure ($P_{id}=\rho T$), as a function of $\rho\sigma$ in the case of $\epsilon=-10$ (squares), $\epsilon=0$ (circles), and $\epsilon=10$ (triangles), for a system with the same parameters as in Fig. 4. The solid lines are the corresponding analytical values obtained according to formula (20).

MD simulations. The agreement between theory and numerical experiments is satisfactory for the three possible cases: attractive, repulsive, and vanishing interparticle interactions. The virial formula (35) is employed to compute the pressure of the system by averaging over different MD runs. The simulated pressure values are plotted, in Fig. 5, together with those obtained by a self-consistent solution of formula (20) with the appropriate replacement of the heat-bath temperature T by the granular temperature T_g , Eq. (37).

The use of formula (20) implicitly assumes that the pair-correlation function for the inelastic model maintains the same functional dependence as its equilibrium counterpart. Such a hypothesis can be checked by measuring during MD runs the three collision frequencies ω_0 , ω_+ , and ω_- and comparing them with their theoretical prediction. The behavior of these quantities with the dimensionless variable $\rho\sigma$ is reported in Fig. 6, for both attractive and repulsive interactions. Even in the inelastic case, one observes that the ratio, ω_0/ω_+ , between frequencies of dissipative collisions and barrier crossing increases with density from the value of 1, observed in a very diluted system, as shown in Fig. 7. This is very consistent with the prescription provided by formula (32) that, hard-core collisions, in this model, become dominant events at higher densities.

In the case of barriers [Fig. 6(a)], the theoretical frequencies agree fairly with those extracted from simulations. However, some discrepancies arise when particles may mutually attract [Fig. 6(b)], even though the overall trend of the frequencies with the particle density is correctly captured by the theoretical predictions. The differences induced by inelasticity become more evident in Fig. 8, where we plot the theoretical and numerical pair-correlation functions $g(y)$ at the value $\rho\sigma=0.05$ for repulsive (c) and attractive (d) particles. Again, the theory fits faithfully the simulations for the system with repulsive interactions, while, for attracting particles, the simulated $g(y)$ deviates of about a factor 2 from its estimate in the interval $\sigma \leq y \leq b\sigma$. Figures 8(a) and 8(b), on the contrary, indicates clearly that our theoretical approach perfectly describes the functions $g(y)$ of the elastic system with both attractive and repulsive forces.

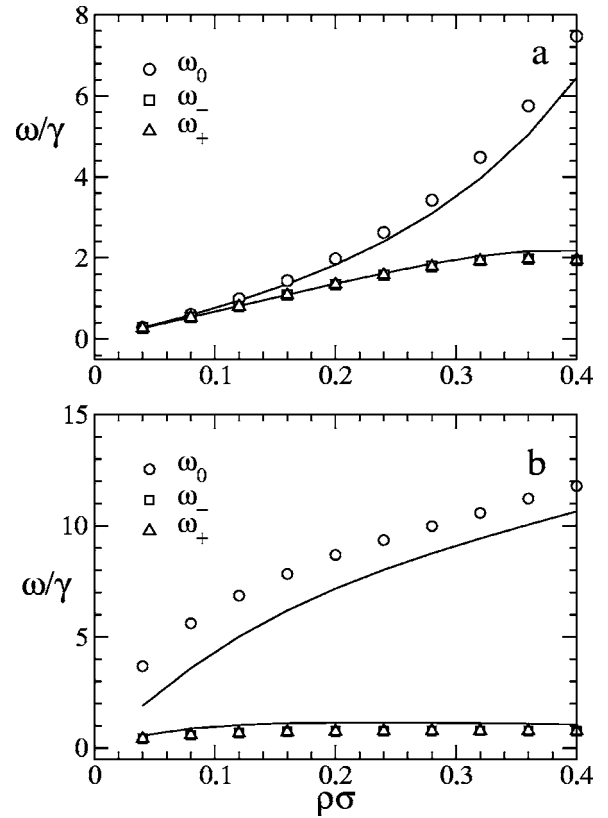


FIG. 6. Collision frequencies at particle separation $x_{ij}=\sigma$ and $x_{ij}=b\sigma$ as a function of $\rho\sigma$. (a) Shows the repulsive case ($\epsilon=-10$) while (b) refers to attractive interaction ($\epsilon=10$). The lines correspond to the theory from Eq. (28). The remaining parameters are as in Fig. 4.

The difficulty encountered by the theory to fit some regimes of the system with attracting inelastic particles can be ascribed to the different effects that the repulsive and attractive interactions induce on the inelastic system. The former basically entails a system reelasticization which may favor homogeneous particle distributions, while the latter enhances the frequency of inelastic collisions leading to clustering. The relevant physical parameter controlling the system be-

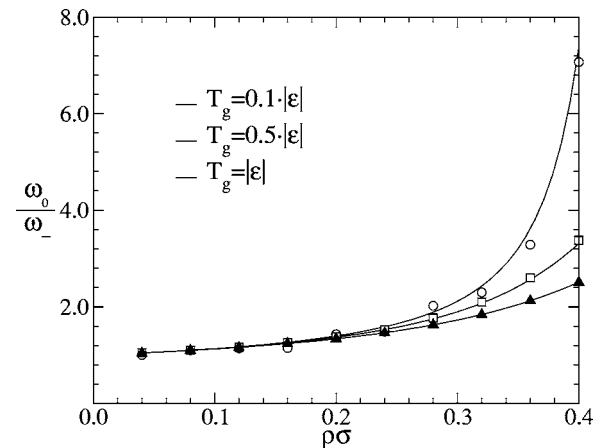


FIG. 7. Collision ratio [Eq. (32)], as a function of $\rho\sigma$ at temperatures $T_g = |\epsilon|$, $T_g=5|\epsilon|$, and $T_g=10|\epsilon|$, for a driven system of $N=2000$ particles with inelasticity $\alpha=0.99$ and a barrier of sizes $b=2$, $\epsilon=-1$ in contact with a bath of viscosity $\gamma=0.2$. Each point is the average over a single run of duration $t_{max}=10^4$, sampled every $t_{sample}=1.0$ time units $=1/\gamma$.

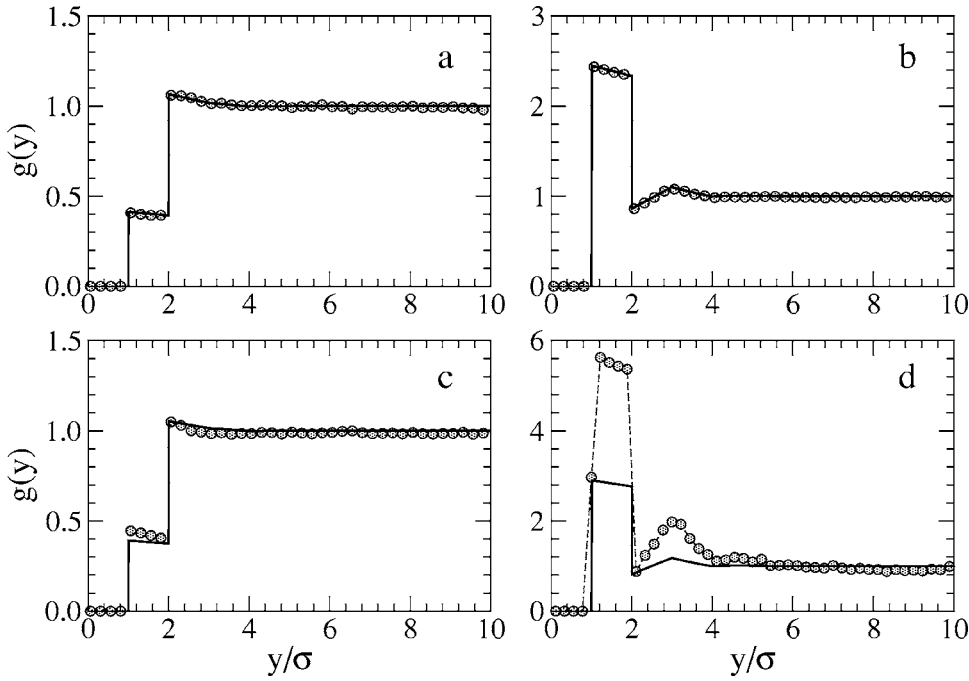


FIG. 8. Simulated (circles) and theoretical (solid line) pair correlations as a function of the rescaled distance y/σ , for system of $N=2000$ hard rods with repulsive-elastic (a), attractive-elastic (b), repulsive-inelastic ($\alpha=0.9$) (c), and attractive-inelastic ($\alpha=0.9$) (d) interactions, and parameters $T=|\epsilon|$, $\epsilon=10$, $\gamma=0.2$, $\rho\sigma=0.05$, and $b=2$. The points represent the average of the function over 10^4 sampled configurations extracted from run of length of $t=10^4$.

havior is the ratio $|\epsilon|/T_g$, thus a good evaluation of T_g is crucial to make accurate theoretical predictions. Our estimate of the granular temperature T_g , from Eq. (37), is based on the assumptions of spatial homogeneity. For repulsive interactions (barriers) the homogeneous state occurs, while for cohesive interactions, particles, under specific conditions, can easily cluster making the system inhomogeneous. If this happens, the single observable, T_g , does not describe properly the kinetic state of the system and, in addition, its estimate from Eq. (37) is incorrect since that formula neglects local temperature fluctuations.

The deviations of the theory from simulations become less pronounced as γ increases, and the reliability of the theoretical approach can be quantified by the integrated difference between numerical, $g_n(y)$, and theoretical, $g_t(y)$,

$$\Delta g = \frac{1}{\sigma} \int_{\sigma}^{b\sigma} dy [g_n(y) - g_t(y)], \quad (38)$$

for various values of γ , but $\epsilon/T=\text{const}$. The dependence of Δg on γ shown in Fig. 9 reflects the fact that the response of the fluid to the action of the heat bath is faster as $\gamma \rightarrow \infty$ and thus erases more rapidly the memory of inelastic collisions. Within this limit one recovers the behavior of the elastic system.

VI. CONCLUSIONS

In this paper we have investigated both theoretically and numerically the influence of a finite range interparticle interaction on the behavior of a one-dimensional inelastic hard-rod system. Forces and interactions whose range is larger than the size associated with the excluded volume constraint are often present in many realistic granular materials. In the specific case, we have chosen a square-well potential to model attraction and a square barrier to model repulsion. These simple shapes, in the case of undriven system, still enable a computer implementation of the particle evolution in terms of a collision driven molecular dynamics. In fact, simple transformations describe the instantaneous changes of velocities when the separation between two particles corresponds to the two characteristic ranges of the potential. We first analyzed how the interplay between these finite range forces and inelasticity modifies the cooling scenario with respect to the free inelastic system. We found that in the case of repulsive barriers the temperature decay becomes slower than Haff's $1/t^2$ power law and eventually reaches a regime where the system is nearly elastic. In the case of attractive wells, instead, the granular temperature is lost faster than an inverse time power law.

Second, we studied the behavior of the stationary regime obtained through a stochastic forcing of the system. The

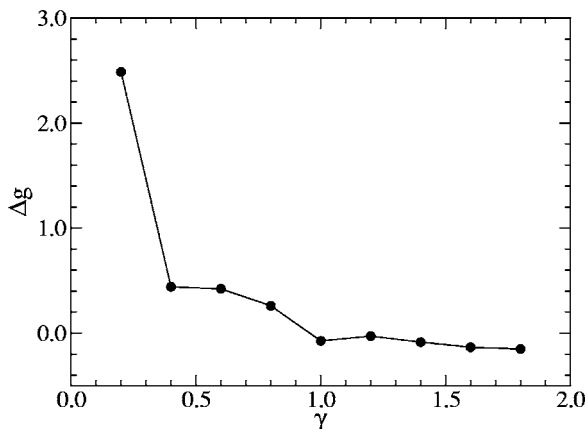


FIG. 9. Parametric plot of the cumulated difference Δg between theoretical and simulated correlations function [see Eq. (38)] vs the friction coefficient γ , for an inelastic system with $N=2000$ rods and parameters $\alpha=0.9$, $T=10$, $\epsilon=10$, $\rho\sigma=0.05$, and $b=2$.

steady state has been analyzed via MD simulations and theoretical approaches based on the direct comparison with the elastic counterpart of the system whose equilibrium properties are well understood. Our results show that, in the dense limit, particle spatial correlations are relevant and modify the collision rate, the excluded volume of the other particles enhances the probability that two particles are at contact and thus reduce the repulsive barrier. The theoretical approach we have attempted remains a reliable approximation for the behavior of the dissipative system at not too small densities while it is correct for the elastic system at every density.

ACKNOWLEDGMENT

One of the authors (U.M.) acknowledges the financial support of the Project Complex Systems and Many-Body Problems Cofin-MIUR 2003 prot. 2003020230.

- ¹*Granular Gas Dynamics*, Lectures Notes in Physics Vol. 624, edited by T. Pöschel and N. Brilliantov (Springer-Verlag, Berlin, 2003), and references therein.
- ²L. P. Kadanoff, *Rev. Mod. Phys.* **71**, 435 (1999).
- ³H. M. Jaeger and S. R. Nagel, *Science* **255**, 1523 (1992).
- ⁴H. M. Jaeger, S. R. Nagel, and R. P. Behringer, *Rev. Mod. Phys.* **68**, 1259 (1996).
- ⁵I. Goldhirsch, *Annu. Rev. Fluid Mech.* **35**, 267 (2003).
- ⁶M. Schultz, B. M. Schultz, and S. Herminghaus, *Phys. Rev. E* **67**, 052301 (2003).
- ⁷T. Scheffler and D. E. Wolf, *Granular Matter* **4**, 103 (2002).
- ⁸T. C. Halsey and A. J. Levine, *Phys. Rev. Lett.* **80**, 3141 (1998).
- ⁹D. Blair and A. Kudrolli, *Phys. Rev. E* **67**, 021302 (2003).

- ¹⁰S. McNamara and W. R. Young, *Phys. Fluids A* **4**, 496 (1992); **5**, 34 (1993).
- ¹¹N. Sela and I. Goldhirsch, *Phys. Fluids* **7**, 507 (1995).
- ¹²Y. Du, H. Li, and L. P. Kadanoff, *Phys. Rev. Lett.* **74**, 1268 (1995).
- ¹³D. R. M. Williams and F. C. MacKintosh, *Phys. Rev. E* **54**, R9 (1996).
- ¹⁴A. Baldassarri, U. Marini-Bettolo-Marconi, and A. Puglisi, *Europhys. Lett.* **58**, 14 (2002).
- ¹⁵B. J. Alder and T. E. Wainwright, *Phys. Rev. A* **1**, 18 (1970).
- ¹⁶P. K. Haff, *J. Fluid Mech.* **134**, 401 (1983).
- ¹⁷A. Puglisi, V. Loreto, U. Marini-Bettolo-Marconi, A. Petri, and A. Vulpiani, *Phys. Rev. Lett.* **81**, 3848 (1998).
- ¹⁸A. Puglisi, V. Loreto, U. Marini-Bettolo-Marconi, and A. Vulpiani, *Phys. Rev. E* **59**, 5582 (1999).
- ¹⁹H. Takahashi, *Proc. Phys. Math. Soc. Jpn.* **24**, 60 (1942).
- ²⁰M. Bishop and M. A. Boonstra, *Am. J. Phys.* **51**, 564 (1983).
- ²¹To the best of our knowledge the pair-correlation function for the one-dimensional hard-rod fluid had not been obtained previously.
- ²²F. Zernike and J. A. Prins, *Z. Phys.* **41**, 184 (1927).
- ²³Z. W. Salsburg, R. W. Zwanzig, and J. G. Kirkwood, *J. Chem. Phys.* **21**, 1098 (1953).
- ²⁴M. Plischke and B. Bergersen, *Equilibrium Statistical Physics*, 2nd ed. (World Scientific, Singapore, 1994).
- ²⁵J. Karkheck and G. Stell, *Phys. Rev. A* **25**, 3302 (1982); *J. Chem. Phys.* **75**, 1475 (1981).
- ²⁶I. P. Omelyan and M. V. Tokarchuk, *Physica A* **234**, 89 (1996).
- ²⁷T. P. C. Van Noije and M. H. Ernst, *Granular Matter* **1**, 57 (1998).
- ²⁸F. Cecconi, U. Marini-Bettolo-Marconi, A. Puglisi, and A. Vulpiani, *Phys. Rev. Lett.* **90**, 064301 (2003).
- ²⁹F. Cecconi, U. Marini-Bettolo-Marconi, A. Puglisi, and F. Diotallevi, *J. Chem. Phys.* **121**, 5125 (2004); **120**, 35 (2004).
- ³⁰M. P. Allen and D. J. Tildesley, *Computer Simulation of Liquids* (Clarendon, Oxford, 1987).
- ³¹E. Ben-Naim, S. Y. Chen, G. D. Doolen, and S. Redner, *Phys. Rev. Lett.* **83**, 4069 (1999).
- ³²E. Efrati, E. Livne, and B. Meerson, *Phys. Rev. Lett.* **94**, 088001 (2005).